

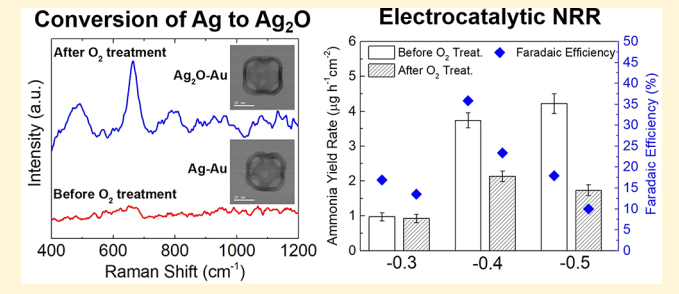
The Role of Oxidation of Silver in Bimetallic Gold—Silver Nanocages on Electrocatalytic Activity of Nitrogen Reduction Reaction

Mohammadreza Nazemi^{†,‡} and Mostafa A. El-Sayed*,[†]

[†]Laser Dynamics Laboratory, School of Chemistry and Biochemistry and [‡]George W. Woodruff School of Mechanical Engineering, Georgia Institute of Technology, Atlanta, Georgia 30332-0400, United States

Supporting Information

ABSTRACT: Electrochemical ammonia synthesis from nitrogen and water provides an alternative route to the thermochemical process (Haber-Bosch) in a clean, sustainable, and decentralized way if electricity is generated from renewable sources. We previously demonstrated the use of bimetallic hollow Au-Ag nanocages as an effective electrocatalyst for electrosynthesis of ammonia in an aqueous solution. The stability of the electrocatalyst during electrochemical nitrogen reduction reaction (NRR) is of paramount importance when considering the feasibility of electrochemical NRR for industrial applications. Here, the role of oxidation of



silver in bimetallic Au-Ag nanocages with various localized surface plasmon resonance peak positions on electrocatalytic activity of NRR is studied by oxygen treatment of Ag through the simple oxidation process to form Ag₂O-Au nanocages. Electrocatalytic NRR activity with an NH₃ yield rate of 2.14 μ g cm⁻² h⁻¹ and Faradaic efficiency of 23.4% was achieved at -0.4V versus reversible hydrogen electrode (RHE) using Ag₂O-Au-719. This electrochemical performance is a substantial reduction to our previously reported NRR activity using Ag-Au-715 nanocages (3.74 μg cm⁻² h⁻¹ and 35.9% at -0.4 V vs RHE). This work highlights the importance of an O₂-free environment in electrochemical NRR for the stable N₂ electrolysis operation and discerns the role of Ag on the selectivity and activity of bimetallic Au-Ag nanocages toward NRR.

INTRODUCTION

Ammonia plays a significant role in producing agricultural fertilizer, energy, and in the pharmaceutical industry. The global production of ammonia was 146 million tons in 2015 and is estimated to increase by 40% in 2050. 2,3 Electrochemical nitrogen reduction reaction (NRR) provides an ideal pathway for clean, sustainable, and decentralized ammonia synthesis. In the conventional thermochemical process (Haber-Bosch process) for ammonia synthesis, N2 and H2 are converted to NH₃ at high operating pressures (150-250 bar) and temperatures (350-550 °C) over iron-based catalysts. 4 This process is responsible for consuming 3-5% of the global natural gas supply, 60% of the worldwide hydrogen production, and emits 450 million metric tons of CO₂ annually.⁵

Developing an effective electrocatalyst that converts N2 to NH₃ with a high yield and Faradaic efficiency (FE) is necessary to further investigate the applicability of electrochemical NRR for sustainable ammonia production. Recently, single atom and hybrid Au electrocatalyst has attracted a great attention due to the strong ability of Au to activate and break N≡N through the associative mechanism where N2 adsorbs on the Au surface with further sequential hydrogenation to form adsorbed N₂H_x species (1 < x < 4) and the rate-determining step is N_2 dissociation (reduction of N2* to form NNH*).6-12 This capability is in line with the weak adsorption of protons on the Au surface in the aqueous media, resulting in higher selectivity for NRR compared with other metallic and metal-free electrocatalysts. 13-16 Also, through the rational design of electrode-electrolyte, superior electrocatalytic NRR activity can be achieved by improving the selectivity of N2 on the electrocatalyst's surface and suppressing proton (H⁺) reduction reaction. 17-19

In our previous study, we demonstrated the use of pore-size controlled bimetallic Au-Ag nanocages with tunable localized surface plasmon resonance (LSPR) peak positions as an effective electrocatalyst in an ionic aqueous solution.²⁰ The interdependency between the pore size/density, the LSPR peak position, the silver content in the cavity, and the electrochemical surface area of the nanoparticle were determined to be the critical factors for improving the electrocatalytic activity of NRR. The chemical stability of the electrocatalyst during electrochemical NRR is essential in further consideration of the catalyst for industrial applications. Here, we aim to investigate the role of oxidation of Ag in bimetallic Au-Ag nanocages by preparing Ag₂O-Au nanocages through the facile oxidation process to mimic the possible oxidation of Au-Ag electrocatalyst at the presence of O₂ in the electrolyte during electrochemical NRR. This work also

Received: February 3, 2019 Revised: April 12, 2019 Published: April 16, 2019

discerns the role of Ag on the selectivity and activity of the electrocatalyst toward NRR compared to active sites of Au surface in bimetallic Au–Ag nanocages.

EXPERIMENTAL SECTION

Nanoparticle Synthesis. Silver nanocubes (AgNCs) and Ag—Au nanocages with various LSPR peak positions are prepared by a modified polyol reduction of AgNO $_3$ and galvanic replacement techniques. For O $_2$ treatment of prepared nanoparticles, 5 mL of cleaned nanoparticle (e.g., Ag—Au-635) dispersed in deionized (DI) water is transferred to the glass vial equipped with an inlet and outlet for purging gas. Then, pure O $_2$ gas is bubbled through the glass vial with the flow rate of 20 mL min $^{-1}$ for 6 h. The Ag $_2$ O—Au nanocages with LSPR peak positions at 644 and 719 nm have optical densities (ODs) of 1.4 and 2.4.

Electrochemical Measurement. A Mott–Schottky (MS) plot for Ag_2O nanocubes at a frequency of 1000 Hz was obtained in 0.5 M LiClO₄ aqueous solution under the dark condition. Cyclic voltammograms (CV) of nanoparticles were conducted in the three-electrode setup using a rotating disk electrode.

■ RESULTS AND DISCUSSION

Bimetallic porous Au-Ag nanocages with various LSPR peak positions are prepared by adding HAuCl₄ (aq) solution to the solid silver nanocubes (AgNCs) solution through the galvanic replacement method. 20,21 By oxygenating the Au-Ag nanocages through purging the solution with pure oxygen gas, Ag is oxidized to form silver(I) oxide (Ag₂O) at room temperature, an extremely stable metal oxide semiconductor at ambient conditions. After oxygen treatment of the Au-Ag nanocages, the LSPR peak position slightly redshifts (e.g., 9 nm for Au-Ag-635), suggesting the formation of Ag₂O in the cavity and successful synthesis of Ag₂O-Au nanocages (Figure 1A). Furthermore, the surface-enhanced Raman spectroscopy (SERS) spectrum of Ag₂O shows distinct peaks at 460, 685, 817, 964, 1083 cm⁻¹, which are all attributed to the Ag-O vibrational modes (Figure 1B). These peaks with slight shift are observed for Ag₂O-Au nanocages, while no pronounced SERS peak is observed for the Au-Ag nanocages, further confirming the formation of Ag₂O after oxygen treatment of Au–Ag nanocages (Figure 1B).²² The size and density of pores in the walls of hollow Au-Ag nanocages are controlled by tuning their LSPR peak position. By increasing the amount of Au³⁺ ions added to the AgNCs template, Ag atoms are etched and replaced by Au atoms. This results in the LSPR peak position to redshift from 635 to 715 nm and the pore size at the walls and corners of the nanocages to increase (Figure 1C,E). The pore size and morphology of nanocages did not change significantly after the O₂ treatment of Au-Ag nanocages (Figure 1D,F). The detailed information regarding the LSPR peak positions before and after oxygen treatment of bimetallic Au-Ag nanocages and the Au and Ag content of nanoparticles, which are determined by inductively coupled plasma emission spectroscopy (ICPES), are provided in the Supporting Information (Table S1). Here, Ag-Au nanocages with LSPR peak positions at 635 and 715 nm are selected for further study based on our previous work, as Ag-Au nanocages with the LSPR peak position at 795 nm showed the lowest electrocatalytic NRR activity.²⁰

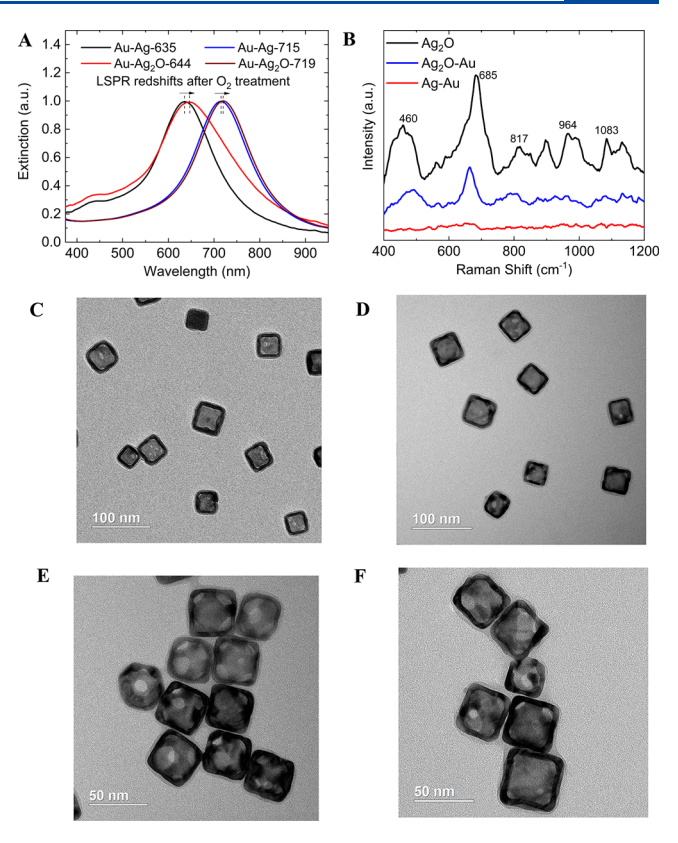


Figure 1. (A) UV–Vis extinction spectra of bimetallic Au–Ag nanocages with various LSPR peak positions before and after O₂ treatment. Before O₂ treatment, the bimetallic Au–Ag nanoparticles have the LSPR peak positions at 635 and 715 nm, while after O₂ treatment the LSPR redshifts to 644 and 719 nm, suggesting the formation of Ag₂O in the cavity (Ag₂O–Au). (B) SERS spectra of Ag₂O, Ag₂O–Au-685, and Ag–Au-670 nanoparticles. The TEM images of bimetallic Au–Ag nanocages with the LSPR peak position (C) at 635 nm before O₂ treatment (Au–Ag-635) and (D) at 644 nm after O₂ treatment (Ag₂O–Au-644). The TEM images of bimetallic Au–Ag nanocages with the LSPR peak position (E) at 715 nm before O₂ treatment (Au–Ag-715) and (F) at 719 nm after O₂ treatment (Ag₂O–Au-719).

Energy-dispersive X-ray (EDX) spectroscopy was performed on single nanocages to determine the shell composition (Figures S1 and S2). 23,24 EDX revealed the O (atom %) content of Au–Ag nanocages increases after $\rm O_2$ treatment (Table S2). Since the areas are selected from the shell of nanocages to determine the surface composition, there is a discrepancy between EDX and ICPES values which are obtained from the bulk analysis. The initial O content before $\rm O_2$ treatment of nanocages is attributed to the chemisorbed oxygen caused by the external – OH group or the water molecule adsorbed on the surface (Table S2).

Cyclic voltammograms of Ag₂O—Au nanocages are obtained in the three-electrode setup using rotating disk electrode (RDE) apparatus in an Ar-saturated 0.1 M LiOH aqueous solution at a rotation rate of 1500 rpm and a scan rate of 50 mV s⁻¹. The peaks observed at potentials around 0.5 V versus reversible hydrogen electrode (RHE) correspond to the reduction of silver(I) oxide in Ag₂O—Au-644 and Ag₂O—Au-719 nanocages. These reduction peaks are slightly larger compared to our previous study using Au—Ag-635 and Au—Ag-715 nanocages, while the reduction peak for Au oxide at potential around 1.2 V versus RHE remained relatively

unchanged (Figure 2A).²⁰ This observation suggests the effective conversion of Ag to Ag₂O after O₂ treatment of

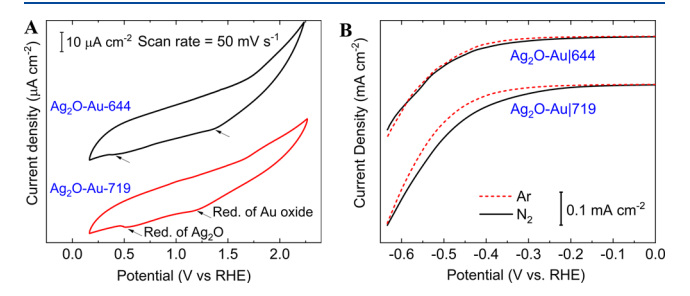


Figure 2. (A) CV of Ag_2O-Au nanocages with various LSPR peak positions in Ar-saturated 0.1 M LiOH aqueous solution at a scan rate of 50 mV s⁻¹. The CV measurements were conducted in the RDE setup at a rotation rate of 1500 rpm at room temperature. (B) LSV tests of Ag_2O-Au with LSPR peak positions at 644 and 719 nm in an Ar- and N_2 -saturated 0.5 M LiClO₄ aqueous solution under ambient conditions with the scan rate of 10 mV s⁻¹.

bimetallic Au–Ag nanocages and successful synthesis of Ag_2O –Au with various LSPR peak positions. This also informs that O_2 treatment of Ag in bimetallic Au–Ag nanocages to form Ag_2O is more effective than electrochemical oxidation of Ag.

Linear sweep voltammetry (LSV) tests are performed in Ar and N₂-saturated 0.5 M LiClO₄ (aq) electrolyte in an H-type cell, where a proton exchange membrane separates anodic and cathodic compartments. A neutral pH electrolyte is selected based on the optimization of electrolyte's pH to obtain the highest electrocatalytic NRR activity. The selectivity performance ($\frac{I_{\rm N_2}-I_{\rm Ar}}{I_{\rm N_2}}$ × 100) of Ag₂O–Au nanocages with

various LSPR peak positions is evaluated toward NRR. Faradaic current is obtained by subtracting the capacitive current from the actual current recorded from LSV tests. For both electrocatalysts, the higher current density was achieved in N_2 -saturated electrolyte compared to Ar-saturated electrolyte within the potential window from -0.2 to -0.5 V versus RHE (Figure 2B). In addition, within this potential window, the selectivity decreases for both electrocatalysts (i.e., $Ag_2O-Au-644$ and $Ag_2O-Au-719$) after O_2 treatment of bimetallic Au-Ag nanocages (Table 1). This clearly reveals the role of Ag

Table 1. Selectivity Performance of Hybrid Plasmonic Nanoparticles with Various LSPR Peak Positions toward NRR

	potential (V vs RHE)		
electrocatalyst	-0.3	-0.4	-0.5
Ag-Au-635	52.3	48.7	45.1
Ag ₂ O-Au-644	46.4	36.7	9.1
Ag-Au-715	55.6	65.3	56.3
Ag ₂ O-Au-719	51.7	48.2	32.1

in promoting the selectivity toward NRR. For instance, at the potential -0.4 V versus RHE, the selectivity decreases from 65.3% to 48.2% after O_2 treatment of Au–Ag-715 nanocages to make Ag₂O–Au-719. If Au atoms were the only active sites for NRR in bimetallic Au–Ag nanocages, the selectivity should remain unchanged after O_2 treatment of Au–Ag nanocages, as Au is a stable metal catalyst even after oxygenation. Since Ag₂O is a p-type semiconductor, at the reduction potentials (e.g.,

-0.4 V vs RHE) for NRR, it acts as a resistor rather than conductor, and therefore it is not an active site for NRR. However, Au atoms serve as primary active sites for NRR, since for all potentials studied, higher selectivity was achieved using Ag₂O-Au-719 compared to Ag₂O-Au-644 (Table 1). This is attributed to the higher Au content in Ag₂O-Au-719 compared to Ag₂O-Au-644, which was revealed by both ICPES and EDX analysis (Tables S1 and S2). It is important to note that, as potential moves from -0.3 to -0.5 V, the selectivity toward NRR decreases from 51.7% to 32.7% for Ag₂O-Au-719 and from 46.4% to 9.1% for Ag₂O-Au-644. Moving toward more negative potentials than -0.6 V, hydrogen evolution reaction (HER) becomes dominant. To determine the Fermi level of Ag₂O and better understand its response to the external applied potential, Ag₂O nanocubes are synthesized by O2 treatment of AgNCs at the LSPR peak position of 445 nm. After O₂ treatment, the extinction spectra dampens, and the LSPR peak position redshifts (11 nm), confirming the formation of Ag₂O nanocubes (Figure 3A).

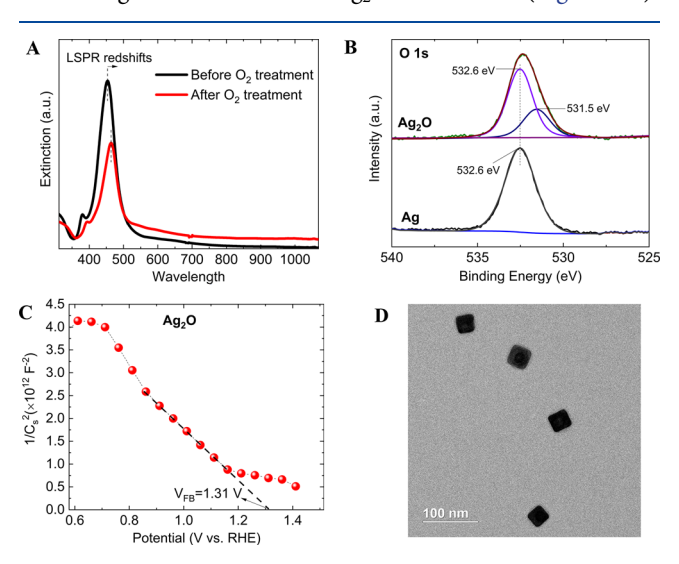


Figure 3. (A) UV–Vis extinction spectra of AgNCs before and after O_2 treatment. (B) O 1s profiles of Ag nanocubes before and after O_2 treatment. All spectra were shift-corrected using a standard reference C 1s, C–C peak at 284.8 eV. (C) MS plot of Ag₂O. An MS plot at a frequency of 1000 Hz was measured in 0.5 M LiClO₄ aqueous solution under the dark condition. (D) The TEM image of solid Ag₂O nanocubes.

Furthermore, the O 1s profile for Ag nanocubes after O2 treatment is deconvoluted into two peaks centered at 531.5 and 532.6 eV, which are attributed to the lattice oxygen atoms of Ag₂O and the chemisorbed oxygen caused by the external -OH group or the water molecule adsorbed on the surface (Figure 3B). 25,26 The latter peak is also observed in the O 1s profile for Ag nanocubes. The MS test is performed to determine the flat band potential $(E_{\rm fb})$ and to confirm the semiconductor type of Ag₂O (Figure 3C). The $E_{\rm fb}$ is determined to be 1.31 V versus RHE. The negative slope of the MS curve confirms that Ag₂O is a p-type semiconductor. At potentials more negative than E_{fb} for a p-type semiconductor such as Ag₂O, depletion region exists, and at potentials more positive than $E_{\rm fb}$ for a p-type semiconductor, accumulation region arises. In the depletion region for Ag₂O (the potential window for NRR is in the depletion region of Ag₂O), there are a few charge carriers available for charge

transfer, and therefore electron transfer reactions happen very slowly. This behavior of Ag_2O is in line with the selectivity performance of Ag_2O-Au -644 and Ag_2O-Au -719 in which by sweeping the potential to more negative potentials (more negative from $E_{\rm fb}$), the selectivity toward NRR continuously decreases (Table 1). The transmission electron microscopy (TEM) image of solid Ag_2O nanocubes reveals the morphology of Ag nanocubes is maintained after the O_2 treatment of nanoparticles (Figure 3D).

Chronoamperometry (CA) tests are performed at -0.4 V versus RHE to determine the ammonia yield rate and FE for Ag₂O-Au-644 and Ag₂O-Au-719 nanocages (Figure 4A,

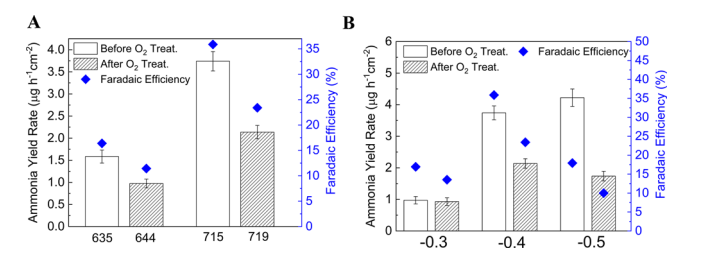


Figure 4. (A) Ammonia yield rate and FE for bimetallic Au–Ag nanocages before and after O_2 treatment with various LSPR peak positions at a potential of $-0.4~\rm V$ vs RHE in 0.5 M LiClO₄ aqueous solution. (B) Ammonia yield rate and FE at various applied potentials in a 0.5 M LiClO₄ aqueous solution.

Figure S3). Furthermore, these results are compared with our previously reported bimetallic Au-Ag electrocatalysts.²⁰ The ammonia yield rate and FE decrease from 1.58 μg cm⁻² h⁻¹ and 16.4% to 0.98 μg cm⁻² h⁻¹ and 11.4% after O₂ treatment of Au-Ag-635 (Figure 4A). Higher ammonia yield rate and FE are obtained using Ag₂O-Au-719 (2.14 µg cm⁻² h⁻¹ and 23.4%) compared to Ag₂O-Au-644, which is consistent with the selectivity performance of these two electrocatalysts for NRR. Again, these results further confirm that, although Ag acts as an active site for NRR, it has lower NRR activity compared to Au atoms. The catalytic activity of Ag₂O-Au nanocages was further compared with solid Au nanoparticles. The higher activity achieved with Ag₂O-Au-719 nanocages even with lower Au content (atom %) compared with pure Au nanoparticles is ascribed to the "cage effect", allowing for the nanoconfinement of nitrogen molecules (Figure S4). In addition, CA tests are performed using Ag₂O-Au-719 to determine the ammonia yield rate and FE at a series of applied potentials (Figure 4B). The same trend is observed for various applied potentials in which the ammonia yield rate and Faradaic efficiency decrease after O2 treatment of bimetallic Au-Ag nanoparticles, with the highest ammonia yield rate and Faradaic efficiency, achieved at −0.4 V versus RHE (Figure 4B).

■ FUTURE OUTLOOK ON ELECTROCHEMICAL NRR

It is essential to compare the input cost in electrochemical NRR (i.e., electricity) method for ammonia synthesis with industrial Haber-Bosch ammonia production process (i.e., natural gas). This helps to better realize the challenges and opportunities for commercialization of green ammonia synthesis through electrochemical NRR. Detailed cost analysis of these two methods including capital and operation and maintenance cost is beyond the scope of this work. The amount of electricity that is required to produce a ton of

ammonia (1000 kg ammonia) is determined based on the highest electrocatalytic NRR activity our group has achieved (NH₃ yield rate = $3.74 \ \mu g \ cm^{-2} \ h^{-1}$, FE = 35.9% at $-0.4 \ V$ vs RHE) according to the following equation:

$$E_{\text{elec}} = \frac{i \times V \times t \times 2.78 \times 10^{-10}}{\text{NH}_3 \text{ yield rate} \times t \times A}$$
 (1)

where i is the avearge current denisty during CA test (49.2 \times 10^{-6} A), V is the full cell potential (1.1 V), t is the operation time (12 h or 12×3600 s), A is the electrode area (1 cm²), and 2.78×10^{-10} is the conversion factor from joules to megawatt hours. This leads to an ~13.4 MWh electricity to make a ton of ammonia. We believe further enhancement in NH₃ yield rate and efficiency could be achieved through the rational design of electrode-electrolyte to decrease the amount of electricity consumption. In the Haber-Bosch process, ~1000 m³ (35 314.7 ft³) of natural gas is needed to make 1 ton of ammonia. With respect to the price volatility of natural gas throughout the year, the input cost of natural gas to make a ton of ammonia is \$143 \pm 13.8 (U.S. natural gas industrial price is taken from U.S. Energy Information Administration (EIA) report). This suggests that green ammonia synthesis is only cost competitive with the Haber-Bosch process if the renewable electricity price is less than \$11 per MWh or 1.1 cent per KWh (Figure 5). This is an optimistic but realistic target to achieve this electricity price from renewable sources such as solar and wind from the current price of ~4-5 cents per kWh.

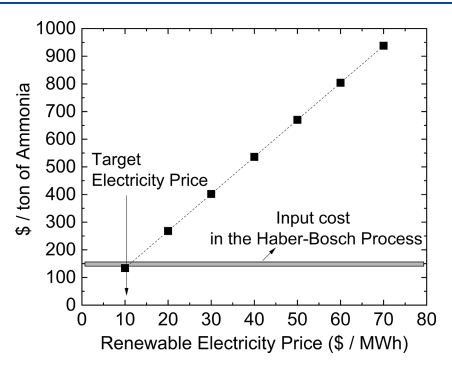


Figure 5. Input electricity cost for making 1 ton of green ammonia as a function of renewable electricity price. The input natural gas cost for making a ton of ammonia in the Haber-Bosch process is relatively constant, while for green ammonia there is a substantial room to decrease the renewable electricity price and therefore be cost competitive with the Haber-Bosch process.

CONCLUSIONS

Electrochemical nitrogen fixation offers an ideal route for clean, sustainable, and decentralized ammonia synthesis and can be an alternative pathway for the Haber-Bosch process if the price of electricity from renewable sources such as solar and wind decreases to ~1 cent per kWh. In addition, the chemical stability of the electrocatalyst during electrochemical NRR was evaluated by preparing Ag₂O-Au nanocages with two LSPR peak positions at 644 and 719 nm through the O₂ treatment of bimetallic Au-Ag nanocages. Electrocatalytic NRR activities of both Ag₂O-Au-644 and Ag₂O-Au-719 nanocages are lower than those of Au-Ag-635 and Au-Ag-715, suggesting the role of Ag in promoting the selectivity and

activity for NRR. It was also observed that Au has higher activity toward NRR compared to Ag, as by redshifting the LSPR from 644 to 719 nm, the electrocatalytic NRR activity increased. This is attributed to the higher Au content in Ag_2O-Au -719 nanocages compared to Ag_2O-Au -644. This work emphasizes the importance of an O_2 -free electrolyte and careful synthesis and treatment of bimetallic Au-Ag nanocages to avoid the formation of Ag_2O in the cavity, which causes a significant reduction in electrocatalytic NRR activity.

ASSOCIATED CONTENT

Supporting Information

The Supporting Information is available free of charge on the ACS Publications website at DOI: 10.1021/acs.jpcc.9b01107.

Chemicals and materials, working electrode preparation, electrochemical measurement, nanoparticles' concentration, and instrumentation (PDF)

AUTHOR INFORMATION

Corresponding Author

*E-mail: melsayed@gatech.edu.

ORCID 6

Mohammadreza Nazemi: 0000-0002-1735-9277 Mostafa A. El-Sayed: 0000-0002-7674-8424

Notes

The authors declare no competing financial interest.

ACKNOWLEDGMENTS

This material is based upon work suppported by National Science Foundation, Division of Chemistry, CHE-1608801. Materials characterization was performed at the Georgia Tech Institute for Electronics and Nanotechnology, a member of the National Nanotechnology Coordinated Infrastructure, which is supported by the National Science Foundation (Grant No. ECCS-1542174). The authors would like to thank T. Brown for helpful discussions on the cost analysis of ammonia production systems. The authors acknowledge financial support from the TI:GER program at the Georgia Institute of Technology.

REFERENCES

- (1) Smil, V. Detonator of the population explosion. *Nature* **1999**, 400, 415.
- (2) Survey, U. G.; S, O.; Survey, U. G. Mineral Commodity Summaries, 2009; Government Printing Office, 2009.
- (3) Economic, U. N. D. o. World population prospects: The 2006 revision; United Nations Publications, 2007; Vol. 261.
- (4) Smil, V. Enriching the earth: Fritz Haber, Carl Bosch, and the transformation of world food production; MIT press, 2004.
- (5) Strait, R.; Nagvekar, M. Carbon dioxide capture and storage in the nitrogen and syngas industries. Nitrogen + Syngas 2010, 303, 1–3.
 (6) Bao, D.; Zhang, Q.; Meng, F. L.; Zhong, H. X.; Shi, M. M.; Zhang, Y.; Yan, J. M.; Jiang, Q.; Zhang, X. B. Electrochemical Reduction of N₂ under Ambient Conditions for Artificial N₂ Fixation and Renewable Energy Storage Using N₂/NH₃ Cycle. Adv. Mater. 2017, 29, 1604799.
- (7) Shi, M. M.; Bao, D.; Wulan, B. R.; Li, Y. H.; Zhang, Y. F.; Yan, J. M.; Jiang, Q. Au Sub-Nanoclusters on TiO₂ toward Highly Efficient and Selective Electrocatalyst for N₂ Conversion to NH₃ at Ambient Conditions. *Adv. Mater.* **2017**, *29*, 1606550.
- (8) Wang, X.; Wang, W.; Qiao, M.; Wu, G.; Chen, W.; Yuan, T.; Xu, Q.; Chen, M.; Zhang, Y.; Wang, X.; et al. Atomically dispersed Au1

- catalyst towards efficient electrochemical synthesis of ammonia. *Science Bulletin* **2018**, *63*, 1246–1253.
- (9) Wang, H.; Wang, L.; Wang, Q.; Ye, S.; Sun, W.; Shao, Y.; Jiang, Z.; Qiao, Q.; Zhu, Y.; Song, P.; et al. Ambient Electrosynthesis of Ammonia: Electrode Porosity and Composition Engineering. *Angew. Chem., Int. Ed.* **2018**, *57*, 12360–12364.
- (10) Qin, Q.; Heil, T.; Antonietti, M.; Oschatz, M. Single-Site Gold Catalysts on Hierarchical N-Doped Porous Noble Carbon for Enhanced Electrochemical Reduction of Nitrogen. *Small Methods* **2018**, 2, 1800202.
- (11) Zheng, J.; Lyu, Y.; Qiao, M.; Wang, R.; Zhou, Y.; Li, H.; Chen, C.; Li, Y.; Zhou, H.; Jiang, S. P. Photoelectrochemical Synthesis of Ammonia on the Aerophilic-Hydrophilic Heterostructure with 37.8% Efficiency. *Chem.* **2019**, *5*, 617.
- (12) Yang, J.; Guo, Y.; Lu, W.; Jiang, R.; Wang, J. Emerging Applications of Plasmons in Driving CO2 Reduction and N2 Fixation. *Adv. Mater.* **2018**, *30*, 1802227.
- (13) Chen, G.-F.; Cao, X.; Wu, S.; Zeng, X.; Ding, L.-X.; Zhu, M.; Wang, H. Ammonia electrosynthesis with high selectivity under ambient conditions via a Li+ incorporation strategy. *J. Am. Chem. Soc.* **2017**, *139*, 9771–9774.
- (14) Chen, S.; Perathoner, S.; Ampelli, C.; Mebrahtu, C.; Su, D.; Centi, G. Electrocatalytic Synthesis of Ammonia at Room Temperature and Atmospheric Pressure from Water and Nitrogen on a Carbon-Nanotube-Based Electrocatalyst. *Angew. Chem.* **2017**, *129*, 2743–2747.
- (15) Cui, B.; Zhang, J.; Liu, S.; Liu, X.; Xiang, W.; Liu, L.; Xin, H.; Lefler, M. J.; Licht, S. Electrochemical synthesis of ammonia directly from N 2 and water over iron-based catalysts supported on activated carbon. *Green Chem.* **2017**, *19*, 298–304.
- (16) Liu, Y.; Su, Y.; Quan, X.; Fan, X.; Chen, S.; Yu, H.; Zhao, H.; Zhang, Y.; Zhao, J. Facile Ammonia Synthesis from Electrocatalytic N2 Reduction under Ambient Conditions on N-Doped Porous Carbon. ACS Catal. 2018, 8, 1186.
- (17) Zhou, F.; Azofra, L. M.; Ali, M.; Kar, M.; Simonov, A. N.; McDonnell-Worth, C.; Sun, C.; Zhang, X.; MacFarlane, D. R. Electrosynthesis of ammonia from nitrogen at ambient temperature and pressure in ionic liquids. *Energy Environ. Sci.* 2017, 10, 2516–2520.
- (18) Suryanto, B. H.; Kang, C. S.; Wang, D.; Xiao, C.; Zhou, F.; Azofra, L. M.; Cavallo, L.; Zhang, X.; MacFarlane, D. R. Rational Electrode–Electrolyte Design for Efficient Ammonia Electrosynthesis under Ambient Conditions. ACS Energy Letters 2018, 3, 1219–1224.
- (19) Suryanto, B. H. R.; Wang, D.; Azofra, L. M.; Harb, M.; Cavallo, L.; Jalili, R.; Mitchell, D.; Chatti, M.; MacFarlane, D. R. MoS2 Polymorphic Engineering Enhances Selectivity in the Electrochemical Reduction of Nitrogen to Ammonia. *ACS Energy Letters* **2019**, *4*, 430.
- (20) Nazemi, M.; El-Sayed, M. A. Electrochemical Synthesis of Ammonia from N2 and H2O under Ambient Conditions Using Pore-Size-Controlled Hollow Gold Nanocatalysts with Tunable Plasmonic Properties. *J. Phys. Chem. Lett.* **2018**, *9*, 5160–5166.
- (21) Nazemi, M.; Panikkanvalappil, S. R.; El-Sayed, M. A. Enhancing the rate of electrochemical nitrogen reduction reaction for ammonia synthesis under ambient conditions using hollow gold nanocages. *Nano Energy* **2018**, *49*, 316–323.
- (22) Waterhouse, G. I.; Bowmaker, G. A.; Metson, J. B. The thermal decomposition of silver (I, III) oxide: A combined XRD, FT-IR and Raman spectroscopic study. *Phys. Chem. Chem. Phys.* **2001**, *3*, 3838–3845
- (23) Polavarapu, L.; Zanaga, D.; Altantzis, T.; Rodal-Cedeira, S.; Pastoriza-Santos, I.; Pérez-Juste, J.; Bals, S.; Liz-Marzán, L. M. Galvanic replacement coupled to seeded growth as a route for shape-controlled synthesis of plasmonic nanorattles. *J. Am. Chem. Soc.* **2016**, *138*, 11453–11456.
- (24) Goris, B.; Polavarapu, L.; Bals, S.; Van Tendeloo, G.; Liz-Marzán, L. M. Monitoring galvanic replacement through three-dimensional morphological and chemical mapping. *Nano Lett.* **2014**, 14, 3220–3226.

The Journal of Physical Chemistry C

- (25) Shi, L.; Liang, L.; Ma, J.; Wang, F.; Sun, J. Enhanced photocatalytic activity over the Ag 2 O-gC 3 N 4 composite under visible light. *Catal. Sci. Technol.* **2014**, *4*, 758–765.
- (26) Xu, M.; Han, L.; Dong, S. Facile fabrication of highly efficient g-C3N4/Ag2O heterostructured photocatalysts with enhanced visible-light photocatalytic activity. ACS Appl. Mater. Interfaces 2013, 5, 12533–12540.